# Large-amplitude coherent phonons and inverse Stone-Wales transitions in graphitic systems with defects interacting with ultrashort laser pulses

Felipe Valencia*
*Advanced Materials Department, Instituto Potosino de Investigación Científica y Tecnolòǵica, Camino a la Presa San Jose 2055, San Luis Potosi, Mexico*
*and Dipartimento di Fisica Galileo Galilei, Università degli Studi di Padova, via F. Marzolo 8, 35131 Padova, Italy*

Aldo H. Romero
*CINVESTAV Querétaro, Libramiento Norponiente No. 2000, 76230 Querétaro, Mexico*

Harald O. Jeschke
*Institut für theoretische Physik, Johann Wolfgang Göethe-Universität, Max-Von-Laue-Strasse 1, 60438 Frankfurt/Main, Germany*

Martin E. Garcia
*Theoretische Physik, Fachbereich Naturwissenschaften, Universität Kassel, Heinrich-Plett-Strasse 40, 34132, Kassel, Germany*
*and Center for Interdisciplinary Nanostructure Science and Technology (CINSaT), Heinrich-Plett-Strasse 40, 34132, Kassel, Germany*
(Received 18 April 2006; published 9 August 2006)

The mechanical response of a defective graphene layer to an ultrafast laser pulse is investigated through nonadiabatic molecular dynamics simulations. The defects are pentagon-heptagon pairs introduced by a single Stone-Wales transformation in the simulation cell. We found that when the fraction of excited electrons $\xi$ is below 6%, the layer exhibits strong transversal displacements in the neighborhood of the defect. The amplitude of these movements increases with the amount of energy absorbed until the threshold of $\xi=6\%$ is reached. Under this condition the layer undergoes a subpicosecond inverse Stone-Wales transition, healing the defect. The absorbed energy per atom required to induce this mechanism is approximately 1.3 eV, a value that is below the laser damage thresholds for the pristine layers. The transition is lead by the electronic entropy and follows a path with strong out-of-plane contributions; it differs from the predicted path for thermally activated transitions, as calculated using standard transition state approaches. The same phenomenon is observed in defective zig-zag and armchair nanotubes. In contrast, for a defective $C_{60}$ fullerene the mechanism is hindered by the presence of edge-sharing pentagons.

DOI: 10.1103/PhysRevB.74.075409 PACS number(s): 61.46.−w, 64.70.Nd, 31.15.Qg

## I. INTRODUCTION

The main goals during the first years of carbon nanotechnology were the production and characterization of novel forms of carbon. As a result of the related experimental and theoretical efforts in that direction, a large variety of nanostructured carbon allotropes has been realized.[1–5] Although different hybridizations may appear in nanostructured carbon-based materials, networks with $sp^2$ hybridization (fullerenes, nanotubes, onions, etc.) are especially attractive because of their mechanical, electronic, and catalytic properties. From the theoretical point of view, these structures are also particularly appealing; many of their properties can be rationalized by analogy or contrast with the simple structure of graphite crystal and graphene layers.[5,6] Carbon nanostructures display a strong interplay between electronic and structural properties.[6] Profound alterations in the behavior of hypothetical devices may be expected from the presence of structural defects.[7] Therefore, a major concern with controlling the structure of the final products has arisen;[5,7] defects appearing during the production stage have to be dealt with, either by annealing them or by introducing them in targeted sites of the structure. Although in general pristine structures are thermodynamically more stable than their defective counterparts, relatively large energetic barriers make the defects metastable at normal laboratory conditions.[8,9] Heating the system to high temperatures can provide the kinetic energy necessary to overcome these barriers but may result in other undesirable structural transformations.

In this paper we focus on graphitic lattices modified by the $\frac{\Pi}{2}$ rotation of one single dimer. This kind of structural modification, known as Stone-Wales (SW) transformation,[8,9] introduces pentagon-heptagon pair defects in otherwise homogeneous hexagonal lattices like nanotubes or graphene layers. In more general graphitic networks (containing rings of sizes other than six), the SW transformation changes the size of the carbon rings neighboring the rotated dimer. In the buckminster fullerene $C_{60}$, a SW mechanism transforms two pentagons into two hexagons and vice versa.

In addition to the pentagon-heptagon pairs appearing regularly in graphitic lattices, SW transformations are believed to be relevant in a broad class of processes, including diffusion,[9] hydrogen adsorption,[10] coalescence in fullerenes,[8,9,11] and nanotubes,[12] and even in the annealing of general fullerene structures down to the buckminster fullerene.[9,13] Typically, transition barriers higher than ~5 eV

 

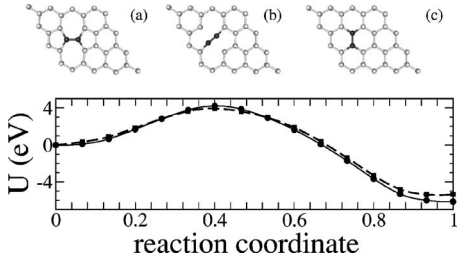


FIG. 1. Top panel: snapshots of the minimum energy path calculated for an inverse SW transition in graphene using the CI-NEB method. (a) The defective system with pentagon-heptagon pairs; (b) transition state exhibiting sensible compression of the rotated dimer; and (c) perfect graphene layer. Bottom panel: The corresponding potential energy along the CI-NEB transition path calculated with the BLYP approximation (circles), and the tight binding energies calculated along the BLYP-based CI-NEB path (squares); the lines are guides to the eye. The calculations were performed using a cluster model saturated with hydrogen atoms (not shown in the picture).

(Refs. 8–10, 13, and 14) have to be overcome in order to go from a homogeneous system to its SW modified counterpart (direct transformation), although catalysis with adsorbed carbon atoms can reduce the barriers significantly through Frenkel pair generation.[15]

The inverse transformation going back from a defective structure to the homogeneous one has been less intensively studied. Under thermal conditions, the systems cannot go back through the direct transition path by overcoming transition barriers that are typically higher than 1.5 eV. For graphite, the barrier could be nearly 4 eV (see Fig. 1). As mentioned above, under these conditions thermal processing may lead to undesirable structural transformations; therefore, it is relevant to explore mechanisms allowing for more controlled exploration of these thermodynamically expensive paths. Irradiation with ultrashort laser pulses has been demonstrated to serve this purpose.[16–19]

As a matter of fact, ultrashort laser irradiation has been shown to be a convenient way to induce structural modifications like ablation, fragmentation, dissociation, and phase transitions in graphitic and other covalent systems.[20–26] This possibility is related to significant changes in the free energy surface of the system due to electronic excitations.[17,27,30,31] Even while typical laser wavelengths are large compared to the nanometer scale, modifications at very short length scales can be achieved. Theoretical evidence suggests the possibility of cleaning up certain kinds of defects in nanotubes.[7,29]

The theoretical description of the interaction between nanostructured materials and realistic ultrashort laser pulses requires several approximations. Higher level approaches like the time-dependent density functional theory (TDDFT) allow for accurate description of the excited states of the system, its energy absorption, and mechanical response.[7] However, the standard TDDFT implementation, the time-dependent local density approximation (TDLDA), is not capable to handle the surface crossing events. Moreover, it artificially keeps too much coherence in the system for longer times and does not give the proper convergence to a thermal electron distribution. Free energy calculations using static density functional theory (DFT) and fixed electronic temperatures provide satisfactory descriptions of massive excitations.[16,30] Fixing the electronic temperature, however, prevents the examination of the system evolution during the laser irradiation time. Simulations based on tight-binding approaches have been shown to provide reliable qualitative descriptions, provided that a suitable description for absorption processes is employed.[20,21,27,28]

In this contribution, we study the mechanical response of defective graphitic lattices under ultrashort laser irradiation using a molecular dynamics scheme based on the tight-binding approximation.[27] The case of a graphene layer with a pentagon-heptagon pair defect is carefully examined. Depending on the amount of energy absorbed from a pulse of $\sim$200 fs duration, we observe strong oscillations on a time scale of the order of $10^2$ fs, and at a given threshold intensity, an inverse Stone-Wales transition leading to defect healing. This mechanism is also observable in zig-zag and in armchair nanotubes.[29] For the buckminster fullerene, the SW transformation creates adjacent pentagons and the inverse transformation is prevented.

In order to get a better understanding of the phenomenon, we contrast this healing mechanism with the thermally induced, inverse Stone-Wales transformation.

In Sec. II we briefly describe the calculation framework we used. Section III reviews the problem of the inverse SW transition in the defective graphene layer on the basis of a transition state analysis, i.e., the thermally activated transition. Section IV reports on the effects of laser irradiation in a single, defective, graphene layer. In Sec. V we show that the laser mechanism is also useful for nanotubes, a fact that was discussed in a previous communication.[29] Section VI deals with the impossibility of an inverse SW transition in $C_{60}$.

## II. CALCULATION METHOD

The fundamentals of the nonadiabatic molecular dynamics approach used in this work have been discussed elsewhere,[20,27] and here we just present a short review of the major concepts.

The electronic system is described using the tight-binding Hamiltonian,

$$H(\{R_i\}) = \sum_{i\eta} \epsilon_{i\eta} c_{i\eta}^{+} c_{i\eta} + \sum_{i\eta,j\eta'} t_{i\eta j\eta'} c_{i\eta}^{+} c_{j\eta'}, \qquad (1)$$

where $c_{i\eta}^{+}(c_{i\eta})$ stands for creation (annihilation) operators of electrons in the atomiclike orbital with a given symmetry $\eta=\{s,p_x,p_y,p_z\}$ localized at the atomic site $i$, $\epsilon_{i\eta}$ is the on-site energy for that orbital, and $t_{i\eta j\eta'}$ is the hopping parameters. We have chosen the tight binding parameters as given by Xu *et al.*,[32] because they provide a good compromise between the mechanical and electronic properties in a wide range of carbon structures. The ions move on a free energy surface, given by the total electronic energy $E_{band}$, a functional form describing the repulsive energy $\Phi(\{R_i\})$ depending on the ionic positions, and the contribution from the electronic entropy,

$$U = E_{band}(\{R_i\}) + \Phi(\{R_i\}) - T_e(n_l)S_e(n_l) \quad (2)$$

where, as usual, the electronic energy is given by the eigenenergies $E_m$ of the Hamiltonian and the corresponding occupation numbers $n(E_m)$,

$$E_{band} = \sum_m n(E_m)E_m.$$

The electronic occupation number varies in time according to the energy absorbed from the pulse,[26]

$$\frac{\partial n_{\epsilon_l}}{\partial t} = \int_{-\infty}^{\infty} d\omega' g(\omega',t)[n_{\epsilon_l-\omega+\omega'}(t) - n_{\epsilon_l}(t) + n_{\epsilon_l+\omega+\omega'}(t) - n_{\epsilon_l}(t)] + \left[\frac{\partial n_{\epsilon_l}}{\partial t}\right]_{col}, \quad (3)$$

where $g(\omega')$ stands for the Fourier representation of the laser pulse envelope function, which we assume to be Gaussian. The $\left[\frac{\partial n_{\epsilon_l}}{\partial t}\right]_{col}$ term provides a phenomenological description of the thermalization of the electronic occupations due to electron-electron collision, and electron-lattice interaction. These processes are described using two decay times, $\tau_{ee}$ and $\tau_{el}$. We used for these calculations $\tau_{ee}$=50 fs and $\tau_{el}$=4.4 ps, which are reasonable values according to pump-probe experimental data on the carrier relaxation process in graphitic systems.[33] Our focus is on processes occurring on time scales of hundreds of femtoseconds, and therefore the results are not very sensitive to changes in those two parameters.

Molecular dynamics simulations with supercells containing $N$=96 and $N$=200 atoms for the graphene layer, $N$=240 atoms for a (12, 0) nanotube, and $N$=252 for a (7, 7) nanotube were performed. Periodic boundary conditions are considered, with two possible scenarios: material samples larger than the laser spot, where expansion can only occur at the sound velocity and therefore on time scales much larger than those considered here, are simulated using fixed supercell boundary conditions; material samples smaller than the laser spot can undergo rapid expansion and are simulated using variable supercell conditions.[26] In each case the equations of motion are integrated using time steps of 0.1 fs.

For the determination of thermal energy barriers and transition paths, we performed *ab initio* calculations within the DFT framework, using the Becke-Lee-Yang-Parr (BLYP) form of the exchange-correlation functional[34,35] (as implemented in the CPMD package[36]). The climbing image nudged elastic band (CI-NEB) method[37,38] was used to achieve good enough estimates of the minimum energy paths. In each case, we used 16 images of the system along the minimum energy path between the pristine and SW-transformed systems. These images were optimized until the sum of the spring and real forces reached the threshold of 0.05 eV/Å.

## III. POTENTIAL ENERGY SURFACE ALONG INVERSE SW TRANSITIONS IN GRAPHENE

Given a potential energy surface (PES), the most probable path between two states is given by the path along the lowest energy barrier, usually referred to as minimum energy path (MEP). Methods like the CI-NEB employed in this work attempt to identify the MEPs and the corresponding transition states (the state with highest energy in the MEP). The MEP path and transition state calculated within CI-NEB for the SW-transformed graphene layer are shown in Fig. 1. This path does not differ fundamentally from the one proposed originally by Kaxiras and Pandey[9] for the SW transformation. The transition state is characterized by a marked compression of the dimer bond length. Associated with this compression, we found a high energy barrier of approximately $E_b$=4.1 eV for the inverse SW transition, in good agreement with other estimates reported in the literature.[9,39,40]

This barrier height guarantees metastability of the pentagon-heptagon pairs. Out-of-plane motion of the dimer could reduce the transition barrier by reducing the C-C bond compression. This possibility was already discussed in Ref. 39 within a tight binding approach, revealing only minor changes for the inverse SW transformation barrier. Annealing of these defects was also suggested to occur for nanotubes on picosecond time scales at temperatures around 4000–5000 K.[41] No evidence of inverse SW transitions at room or moderated temperatures has been reported, to the best of our knowledge, and these defects are generally accepted as long-lived species in that temperature regime. Furthermore, the mostly in-plane paths and related barriers, like that in Ref. 9 and in the present work, are widely used as sensible estimates for the actual transition path[40,42] features and only small changes of the activation barrier may be expected from out-of-plane motions.

We have also calculated the potential energy within the tight binding approximation along the DFT-based CI-NEB path to check how likely it is this process occurs in our subsequent molecular dynamics simulations. The height of the barrier is almost the same ($E_b$=3.95 eV). Therefore, this route for defect healing can be disregarded in our study, where lattice temperatures remain below $T_l$=600 K and simulation times are below 2000 fs.

## IV. LASER-INDUCED DYNAMICS OF SW DEFECTIVE GRAPHENE LAYERS

Next we performed molecular dynamics simulations on a defective graphene layer as described in Sec. II. We did not attempt to tune the laser frequency with respect to the electronic states associated with the defect. Instead, we have selected a value of 1.96 eV, well within the usual experimental range. The pulse width was set to $\tau$=50 fs, and it reaches its maximum intensity at $t$=100 fs. Thus, the interaction time lasts approximately from $t$=0 to $t$=200 fs. The layer was thermalized to a lattice temperature of $T_l$=300 K before activation of the laser pulse.

Different laser intensities, i.e., different amounts of offered energy, were considered. The actual energy absorbed ($E_a$) by the system depends on the motion of the lattice during laser excitation.[43] Still, for fixed width and frequency, there is a monotonic correspondence between the laser intensity and the absorbed energy. In what follows we state our discussion in terms of $E_a$, rather than the laser intensity. We

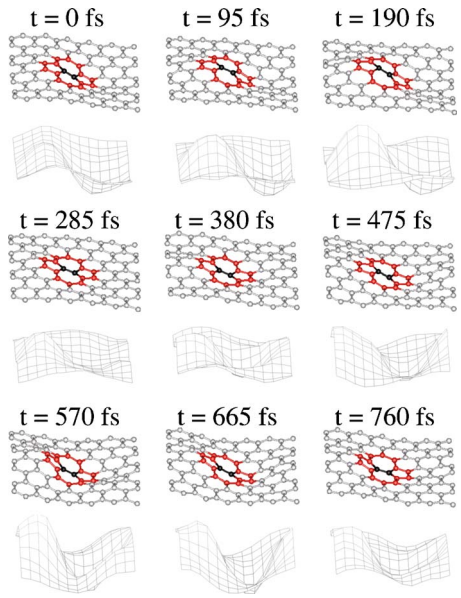


FIG. 2. (Color online) Snapshots of the defective graphene layer response to a Gaussian-shaped laser pulse with $\tau=50$ fs full width at half maximum, centered at $t=100$ fs. The absorbed energy is $E_a=0.77$ eV/atom, and the corresponding fraction of excited electrons $\xi=4\%$. The rotated dimer is shown in black, and the pentagon-heptagon pair defect is highlighted in dark gray (red online). The amplitude of the out-of-plane component of the motion increases during the interaction time and reaches its maximum height at $t=190$ fs. In the net surfaces drawn below each snapshot, the visibility of this out-of-plane component is enhanced.

have found that damage occurs for absorbed energies above $E_a=1.45$ eV/atom, in the case of the $N=96$ atoms supercell, and above $E_a=1.75$ eV/atom for the $N=200$ atoms supercell. The difference in the damage thresholds for the two simulation cells is related to the density of defects; the $N=200$ atoms supercell resembles more closely the pristine graphene layer and thus exhibits a higher damage threshold.[20] At the considered absorbed energies, a significant fraction of electrons, between $\xi=4\%$ and 6%, get promoted to excited states. Correspondingly, the electronic temperatures rise to $T_e=25\,000$ K.

The excitation of coherent phonons in pristine graphite, following laser irradiation, has been discussed in Ref. 44. Here we observe a similar mechanism for the defective layer. In Fig. 2 we show some snapshots for the response of the system to the weakest laser pulse considered ($E_a=0.77$ eV). The out-of-plane motions are stimulated following laser irradiation. The maximum displacement occurs at $t=190$ fs, that is, almost at the end of the interaction time. After irradiation the system undergoes a complex motion, suggesting the excitation of different out-of-plane vibrational modes. This suggestion was confirmed by Fourier transforming the power spectra taken from the $z$ component of the velocity autocorrelation function ($z$-VACF). It is important to point out that the total VACF is dominated by the $z$ component. On the other hand, the rotated dimer bond length exhibits high-frequency oscillations (at about 1650 $cm^{-1}$) which might be related to those found in the TDDFT simulations of Miyamoto *et al.*[45]

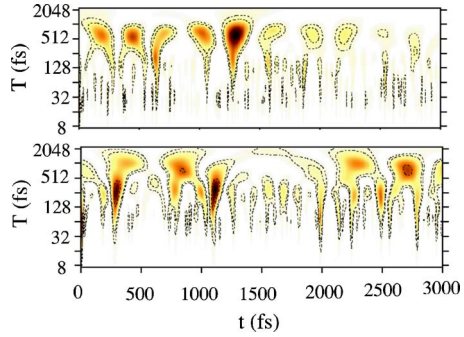


FIG. 3. (Color online) Gray map representation of the squared values of the wavelet coefficients for the $z$-VACF. Top: The free evolution of the thermalized system. Bottom: System irradiated with $E_a=0.77$ eV/atom. The evolution for 3000 fs is depicted.

The transient character of the oscillations limits the amount of information available through the Fourier analysis. In order to examine the underlying periodicity, we applied a multiscale (wavelet)[46–48] analysis to the $z$-VACF. The wavelet analysis is based on the comparison at different times, between the analyzed signal and a test function with a given time scale. The wavelet coefficients are thus given by the convolution

$$C(t,T)=\int dt' f(t')\phi\left(\frac{t'+t}{T}\right), \tag{4}$$

where $f(t')$ is the function to analyze, and $\phi$ is the analyzer *wavelet*, which is relatively well localized in time and frequency. $T$ is referred to as the time scale of the wavelet. The wavelet coefficients, so defined, measure the level of excitation of modes with different frequencies at a given time. However, full resolution in both time and frequency scales should be sacrificed.

We have performed the continuous wavelet transforms of the $z$-VACF using as analyzer the Morlet wavelet,

$$\phi(t,T)=\pi^{1/4}\exp\left(\frac{2\pi it}{T}-\frac{t^2}{2}\right). \tag{5}$$

We choose this wavelet in order to obtain high-frequency resolution and because of its close relation to the Fourier transform.

In Fig. 3 we compare the free evolution of the thermalized system with the evolution upon irradiation ($E_a=0.77$ eV/atom). We obtain the dominant periods of the system by identifying the local maxima of the wavelet coefficients in the time/frequency space, i.e., the intense dots in the wavelet maps. In the first case (upper panel of Fig. 3), the wavelet transform displays features with periods of about $T=570$ fs (the most pronounced), $T=850$ fs, and shorter time scales ($T=8-128$ fs). The amplitude of the coefficients decreases significantly after $t=1500$ fs. Irradiation with the laser pulse excites modes with periods between roughly $T=290$ fs and $T=330$ fs (see the lower panel of Fig. 3). These modes are the most significant feature in the spectra in the time interval between approximately $t=200$ fs and $t=500$ fs (i.e., after the interaction time). A larger period mode is still

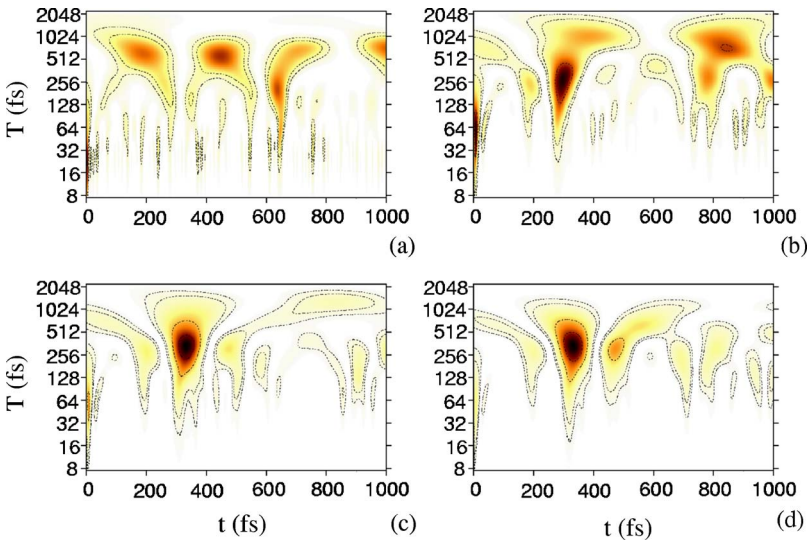


FIG. 4. (Color online) Comparison of the wavelet transforms for (a) the free evolution of the thermalized system; (b) a system irradiated with $E_a=0.77$ eV/atom; (c) a system irradiated with $E_a=1.19$ eV/atom; and (d) a system irradiated with $E_a=1.32$ eV/atom (in which the inverse SW transition takes place). Focus is on the time scale corresponding to the transition times.

present and is responsible for the repetitive pattern with period about $T=850$ fs. After about 2000 fs, the free evolution behavior is recovered.

We did not attempt to find the vibrational eigenmodes for the defective supercell. A simple estimate of the lower frequency modes for the layer can be achieved by considering a continuous model for the graphitic surface. The out-of-plane acoustic modes (labeled *ZA*) for graphene follow a parabolic dispersion relationship,

$$\omega = c_{ZA}|k|^2, \tag{6}$$

where $k$ is the norm of the wave vector, and $c_{ZA} \approx 6 \times 10^{-7}$ m$^2$/s.[49] The periods for the out-of-plane acoustic modes in a rectangular patch with periodic boundary conditions would be given by

$$T_{m,n}^{ZA} = \frac{a^2 b^2}{2\pi c_{ZA}(a^2 m^2 + b^2 n^2)}, \tag{7}$$

where $a$ and $b$ are the linear dimensions of the patch. For the considered cell, $a=14.6$ Å and $b=16.8$ Å). The largest modes supported by the cell would be $T_{0,1}^{ZA}$, $T_{1,0}^{ZA}$, and $T_{1,1}^{ZA}$, with periods of $T=755$ fs, $T=573$ fs, and $T=325$ fs, respectively. A similar estimate for the supported longitudinal and transversal acoustic modes places all their periods below $T=80$ fs. These estimates roughly agree with the periods in the wavelet transform. However, it must be considered that these periods would correspond, at most, to the modes supported by the pristine cell.

The amplitude of the modes at simulation times about $t=300$ fs increases with the absorbed energy, as can be seen in Fig. 4. The highest intensity is achieved for $E_a=1.32$ eV/atom, where the squared value of the coefficient is $|C(t=329\text{ fs}, T=333\text{ fs})|^2=0.15$, compared to $|C(t=271\text{ fs}, T=298\text{ fs})|^2=0.08$ for $E_a=0.77$ eV/atom. The periods of the exited mode change from $T=298$ fs to $T=330$ fs, a fact that might be due to the phonon softening by the laser irradiation. We conclude from the wavelet analysis that the effect of the laser is to strongly enhance the long wavelength vibrations of the graphene sheet and to suppress high frequency modes.

With $E_a=1.32$ eV/atom the system undergoes an ultrafast inverse SW transition, leading to defect healing. Some key steps in this inverse transition path are depicted in Fig. 5:

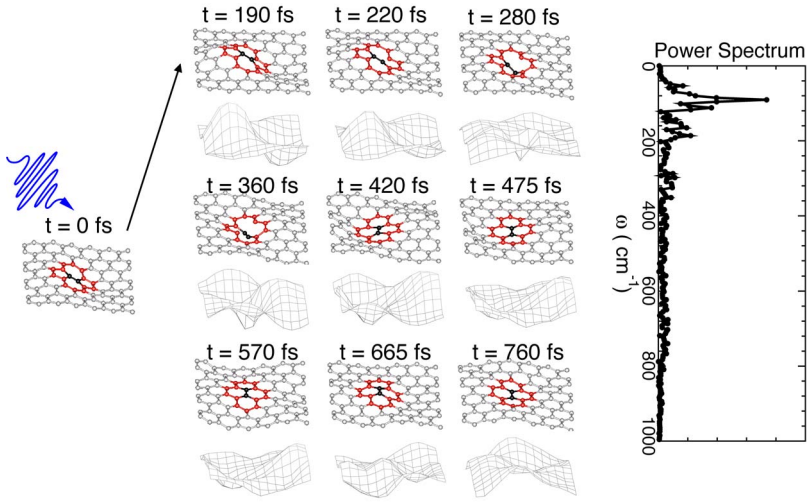


FIG. 5. (Color online) Snapshots for the laser-induced inverse SW transition. When 1.32 eV/atom are absorbed (6% of the electrons are excited), the strong motions are followed by bond breaking, out-of-plane rotation, and finally, defect healing. The rotated dimer is shown in black and the atoms forming the pentagon-heptagon pair defect are shown dark gray (red online). Right panel: The power spectrum taken from the VACF after laser irradiation. Note that the three peaks at low frequency correspond to periods of $T=627$ fs, $T=368$ fs, $T=300$ fs and thus agree well with the wavelet analysis.

strong motions around the defective region are induced after the laser pulse peak (at a time near $t=190$ fs) in a very similar fashion as for lower intensities; out-of-plane motion of the dimer leads to the "liberation" of one of the ends of the dimer (at a time near $t=220$ fs); the dimer moves even further away from the graphite plane and the out-of-plane angle $\beta$ (see definition below) reaches its maximum value (at around $t=280$ fs); the dimer out-of-plane rotation leads to a configuration closely resembling the intimate interstitial-vacancy defect in graphite[40] (at around $t=360$ fs); and finally the defect is annealed and a perfect graphitic lattice is obtained (at around $t=420$ fs). After defect healing the vibrational state of the graphite layer is characterized by the preferential excitation of a well-defined mode, as can be seen from the power spectra in the right panel of Fig. 5. In contrast with the cases for lower fluences, the wavelet coefficients do not recover the thermal behavior, at least not for times below $t=4000$ fs. The period calculated from the power spectrum is $T\approx 368$ fs. The difference between this value and previously mentioned $T=330$ fs is related to the compromise between time and frequency resolution in the wavelet transform.

The out-of-plane motion of the Stone-Wales defect can be further characterized by measuring a dihedral angle $\beta$ between the dimer and two carbon atoms in one neighboring pentagon (if the pentagon were to stay planar that would just be the angle between the dimer and the pentagon plane). Following the evolution of this angle with the absorbed energy we can see (Fig. 6) how the height of the first value reached just after laser irradiation (around $t=220$ fs) changes almost linearly with the absorbed energy. As the laser intensity is increased, the time evolution of the angle gradually changes. But as the intensity reaches the value of defect elimination, we see a qualitative change of the $\beta(t)$ curve, with an early maximum of $\beta\approx 40°$. At this point, one of the edges of the pentagon is broken and the inverse Stone-Wales transition proceeds. After defect healing (at around $t=420$ fs) weak oscillations of this angle can be seen.

Associated with the increase in the amplitude of the vertical displacement and in the maximum value of the dimer angle, there is a sharp increase in the bare potential energy $E_{band}+\Phi$, as can be seen in the bottom panel of Fig. 6. The information in Figs. 2–6 could be interpreted with the help of the simple vibrational modes for the rectangular graphitic patch [Eq. (6)]. The largest phonon modes ($T^{ZA}_{0,1}$ and $T^{ZA}_{1,0}$), providing the long-scale background for the motion, are already active after the thermalization process. These two modes are comprised mainly of wave fronts propagating in directions parallel or perpendicular to the rotated dimer. During the interaction time with the pulse (lasting 200 fs) a mode with shorter period ($T^{ZA}_{1,1}$) is excited. The excitation of this mode results in a rather well-localized perturbation near the dimer. After laser irradiation the layer performs part of an oscillatory motion; at times around $t=280$ fs, the crest of the wave reaches the defective zone. If the intensity of the excited phonon is large enough (compare the snapshots near $t=280$ fs in Fig. 2, and Fig. 5), it can reverse the curvature induced by the defect in the graphene sheet, moving the dimer to a configuration favorable for laser healing; otherwise, the wave is diffracted by the defect, and a complex motion is observed.

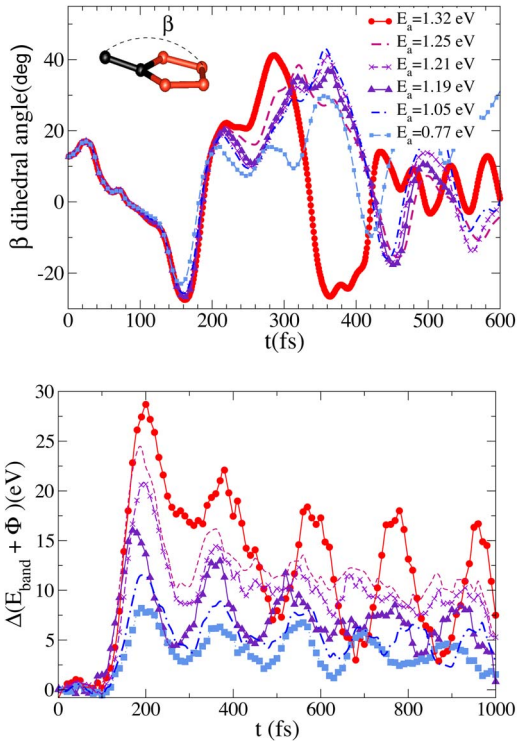


FIG. 6. (Color online) Top panel: Evolution of the dihedral angle between the rotated dimer and an adjacent pentagon with time and absorbed energy. Bottom panel: Bare potential energy profiles along the paths corresponding to different laser intensities, measured with respect to the value at $t=0$ fs. The legend is valid for both panels.

As shown in Fig. 7, this laser-induced path exhibits a very high energy barrier (above $E_b=12$ eV), related to considerable bond stretching during the initial expansion. Therefore, under normal thermal conditions, the system would prefer other paths, like the CI-NEB path discussed above. In Fig. 7 we report the free energy calculated at different constant electronic temperatures. It is clear that by increasing the level

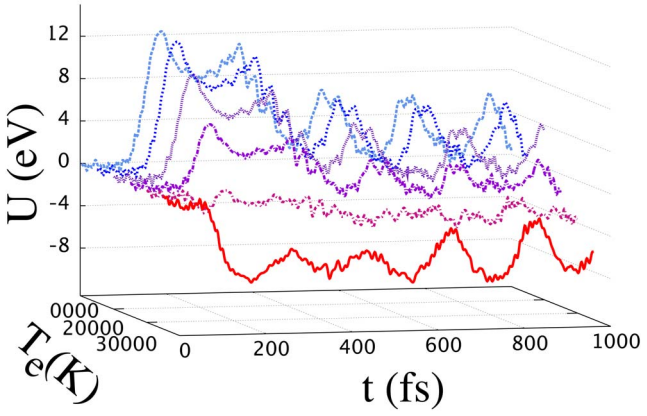


FIG. 7. (Color online) The free energy $U$ that ions would feel moving along the inverse SW transition paths at several electronic temperatures: 300 K, 5000 K, 1000 K, 15 000 K, 20 000 K, and 25 000.

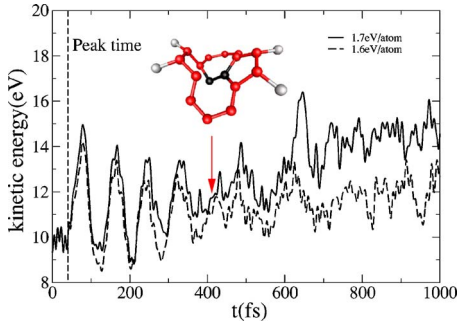


FIG. 8. (Color online) Kinetic energy evolution during the simulation time for a (7, 7) nanotube under laser irradiation for two different values of the absorbed energy. At $E_a$=1.7 eV/atom the inverse SW transition occurs. At $E_a$=1.6 eV/atom the system reaches a metastable state with the dimer pushed into the tube. The configuration of the defect neighborhood at the point where the initial vibrations disappear is also displayed.

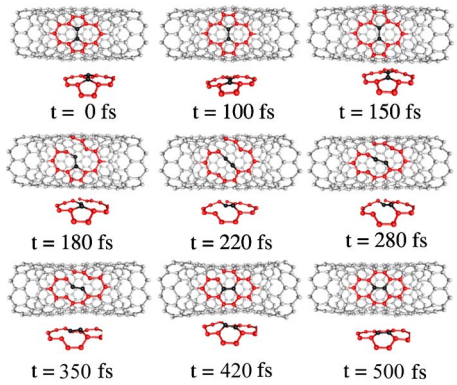


FIG. 9. (Color online) Inverse SW transition in a defective zigzag nanotube. The rotated dimer is shown in black, and the pentagon-heptagon pair defect is highlighted in dark gray (red online).

of electronic excitations (and hence the contribution of the electronic entropic term to the free energy) it is possible to remove the barrier. Therefore, this transition should be regarded as driven by the electronic entropy, a fact that has been discussed earlier in relation to the healing of pentagon-heptagon pairs in carbon nanotubes.[29] A similar analysis using the CI-NEB path showed that it displays a barrier of approximately $E_b$=0.5 eV, even at the higher electronic temperature considered. After healing, the free energy on Fig. 7 exhibits rather well-defined oscillations of period $T \approx 380$ fs, corresponding to the peak observed in the power spectra.

Laser healing with $E_a$=1.32 eV and $\xi$=6% was also observed using a laser pulses with widths of $\tau$=60 fs and $\tau$=40 fs. Before closing this section it is important to mention that a larger energy of $E_a$=1.62 eV/atom is needed in the $N$=200 atoms cell in order to observe the inverse transition. This energy provides roughly the same $\xi$=6% threshold. The period of the phonon mode excited near the transition time is only about $T$=100 fs. Considering that the excited modes in the $N$=96 atoms cell are basically the longest wavelength phonons that fit into our system, this difference in the excited mode could be expected.

## V. ULTRAFAST RESPONSE OF NANOTUBES

The possibility to heal defects in carbon nanotubes is of extreme technological relevance. A rather detailed description of the ultrafast healing of defective armchair nanotubes using ultrashort laser pulses has been presented earlier.[29] Now we illustrate the issue of breathing mode excitation prior to defect healing and explicitly show the inverse transition in zigzag nanotubes.

Figure 8 shows the evolution of the kinetic energy during the simulation time for a defective (7, 7) nanotube like the one described in Ref. 29. From the fluctuations it is clear that the expansion observed in the simulations just after the laser pulse peak (Ref. 29) does correspond to excitation of a vibrational mode with a frequency around 193 $cm^{-1}$. This is not a single mode excitation, as can be seen from the variation in the fluctuation amplitudes. For times above $t$=400 fs this mode is no longer supported by the excited nanotube. As a matter of fact, around $t$=400 fs the out-of-plane component of the SW dimer reaches its maximum value and the dimer breaks free from one of the pentagons. This point in time can be considered the onset for the inverse SW transition.

When the absorbed energy is not enough to efficiently lower the barriers between the break point around $t$=400 fs and the perfect nanotube, the system does not undergo ultrafast transformation and gets stuck in a metastable (only on the simulation time scales) state with the dimer pointing inward. The barrier separating this state from the perfect nanotube should be somewhere below $E_b$=5 eV (the energy barrier at $T_e$=300K), and it is still possible for the system to go to the perfect lattice even if it is not performing a subpicosecond transition.

Snapshots of the laser-induced inverse transition in a defective (12, 0) nanotube are shown in Fig. 9. This path requires $E_a$=1.76eV/atom and $\xi \approx 7\%$. It is important to observe that this trajectory follows the same steps discussed here for the case of graphene, and previously for armchair nanotubes.[29] This fact points to the very general character of the observed phenomena.

Note that a reported first-principles study on photoexcitation of Stone-Wales pairs in carbon nanotubes[45] considers a single electronic excitation aimed to a well-defined electronic state associated with the pentagon-heptagon pair defect. Under such conditions the system was observed to undergo strong and well-determined vibrations at the rotated dimer, without compromising the defect stability. Clearly, these results can be considered as a particular case of the general effect demonstrated here. For low laser intensities, the defected nanotube is still a minimum of the potential surface and the barrier is still large. This means that no ultrafast transition occurs. The SW-type defect continues being metastable with a large lifetime. Our calculations for different laser intensities show that the ultrafast transition (characterized by the elimination of the barrier) requires the excitation of a significant fraction of the valence electrons. For lower intensities, large amplitude anharmonic vibrations around the 7-5-7-5 defect are induced by the laser pulse.

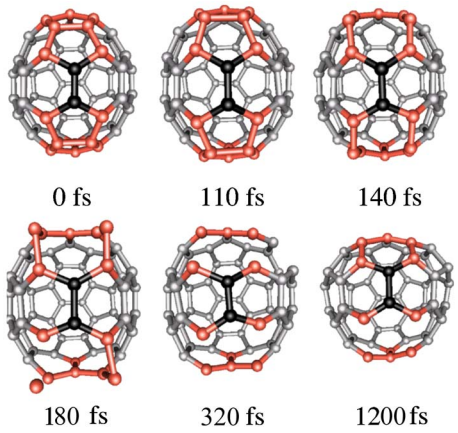


FIG. 10. (Color online) Snapshots from the response of a $C_{2v}$ fullerene to a laser pulse when the absorbed energy is about $E_a$ =1.45 eV/atom with $T_l$=600 K as initial lattice temperature. Emission of 4 atoms is observed followed by structural rearrangement into a smaller cage. The rotated dimer is shown in blue and pentagons in red.

## VI. THE $C_{60}$ FULLERENE

When an SW rotation is performed on the buckminster fullerene, it is transformed into a $C_{2v}$ fullerene having two pairs of adjacent pentagons as shown in Fig. 10. This isomer is a fundamental step in the transformation from any of the 1812 $C_{60}$ fullerenes into the most stable buckminster fullerene. A barrier of about $E_b$=4 eV for the inverse transformation could be expected according to the analysis of Ref. 13.

Thorough simulations with fixed initial temperature ($T_l$=300K), frequency ($\hbar\omega$=1.96 eV), and laser width ($\tau$=50 fs) show a variety of responses. During the initial steps, after laser irradiation, the system undergoes a strong breathing motion, similar to the case of nanotubes and buckminster fullerenes.[28,50] The subsequent evolution time depends on the laser intensity. For low enough absorbed energies (below $E_a$=1.4 eV/atom) the system keeps breathing and reversible breaking of the bond shared by pentagons can occur at this intensity. Above this threshold damage occurs through several mechanisms. Around $E_a$=1.5 eV/atom, several cage windows open through the handles shared by two pentagons or one pentagon and one hexagon, a condition that could be related to ulterior graphitization. Near $E_a$=1.63 eV/atom, emission of atoms and formation of carbon coil chains take place. For energies above $E_a$=1.7 eV/atom fast cage explosion was observed. In each case, bonds shared by two hexagons exhibit more stability that those included in one pentagon. No inverse SW transition was observed.

Changing the initial temperature, frequency, and laser duration does not change the overall results. Taking the initial temperature as $T_l$=600 K, rearrangement of the fullerene into a smaller fullerene after emission of the 4 atoms shared by two pentagons was observed for energies around $E_a$=1.4 eV/atom (see Fig. 10), but still no inverse SW transition was observed.

The existence of adjacent pentagons makes those sites much more unstable under laser irradiation than the SW dimer. Meanwhile, the local neighborhood of the SW dimer is the same in the buckminster and in the C2$v$ fullerenes, meaning that it does feel as comfortable in one or the other isomer. Because of this fact, out-of-plane motion of the dimer, analogous to the tilting discussed for graphene and nanotubes, is not observed. Considering that the inverse transition paths for graphene and nanotubes involve strong inward motion, detaching the dimer from its neighboring atoms, we have tested the energy cost for a similar motion. For that we have modified the trajectory of Fig. 10, pushing one of the atoms in the dimer inward by 0.5 Å, and calculated the free energy for this modified trajectory for times below $t$=140 fs (window opening time) compared with the free energies at each in the original trajectory. The extra energy cost at $T_e$=25 000 K and different trajectory steps varies between 0.5 and 3.0 eV, values that may be regarded as conservative lower bounds for dimer tilting. Tilting the dimer enough to get it detached may be a very expensive step in this fullerene. If the electronic entropy contribution is high enough for the system to overcome this barrier, it is also high enough to break the molecule.

## VII. CONCLUDING REMARKS

The theoretical description of laser healing of defects produced by Stone-Wales transformations in graphene and single walled carbon nanotubes could be achieved using ultrashort pulses. Realization of this healing mechanism would require a careful selection of the laser intensity in order to deposit the right amount of energy into the samples. No fine tuning of the frequency with excited states of the defect may be necessary.

The transition path follows the same trend in the plane graphene and in the nanotubes. Excitation of oscillations in a time scale close to the interaction time was observed as part of the healing mechanism. Therefore, the pulse duration should also be tuned in order to control the process. The key steps in the transition are the same in each case: oscillations, bond breaking with out-of-plane motion of the dimer, and dimer rotation. In this sense, curvature does not change the intrinsic properties of this laser-induced transition, although it should become more important for smaller tubes. The density of defects may play an important part in the ability to heal defects; calculations including two defects in each supercell show that they do not heal simultaneously. The presence of a second defect does not hinder the transition undergone by the first one.

Strong motions are always observed in the regions where the curvature changes. In the case of graphene and the nanotubes, this corresponds to the rotated dimer neighborhood, but for the $C_{60}$ molecule the local curvature in the neighborhood of the dimer is the same as in the pristine fullerene, while adjacent pentagons occur one ring away from the SW dimer. This configuration makes a inverse transition mechanism similar to the one in graphene impractical for the fullerene.

As expected, damage thresholds are significantly reduced in each lattice with respect to the values for pristine structures.

**ACKNOWLEDGMENTS**

M.E.G. acknowledges support by the Deutsche Forschungsgemeinschaft (DFG) through the priority program SPP 1134 and by the European Community Research Training Network FLASH (MRTN-CT-2003-503641). H.O.J. gratefully acknowledges support from the DFG through the Emmy Noether Program. A.H.R. acknowledges support from CONACYT-Mexico under Grant No. J-42647-F. F.V. acknowledges encouraging discussions with A. C. Bernal, Valparaiso, Chile.

*Electronic address: felipevh@pd.infn.it

[1] H. W. Kroto, J. R. Heath, S. C. Obrien, R. F. Curl, and R. E. Smalley, Nature (London) **318**, 162 (1985).
[2] S. Iijima, Nature (London) **354**, 56 (1991).
[3] D. Ugarte, Chem. Phys. Lett. **207**, 473 (1993).
[4] D. L. Dorset and J. R. Fryer, J. Phys. Chem. B **105**, 2356 (2001).
[5] M. S. Dresselhaus and H. Dai, MRS Bull. **29**, 237 (2004).
[6] R. Saito, M. Fujita, G. Dresselhaus, and M. S. Dresselhaus, Appl. Phys. Lett. **60**, 2204 (1992).
[7] Y. Miyamoto, S. Berber, M. Yoon, A. Rubio, and D. Tománek, Chem. Phys. Lett. **392**, 209 (2004).
[8] A. J. Stones and D. J. Wales, Chem. Phys. Lett. **128**, 501 (1986).
[9] E. Kaxiras and K. C. Pandey, Phys. Rev. Lett. **61**, 2693 (1988).
[10] E. J. Duplock, M. Scheffler, and P. J. D. Lindan, Phys. Rev. Lett. **92**, 225502 (2004).
[11] J. Zhao, B. Yakobson, and R. E. Smalley, Phys. Rev. Lett. **88**, 185501 (2002).
[12] M. Yoon, S. Han, G. Kim, S. Lee, S. Berber, E. Osawa, J. Ihm, M. Terrones, F. Banhart, J.-C. Charlier, N. Grobert, H. Terrones, P. M. Ajayan, and D. Tomanek, Phys. Rev. Lett. **92**, 075504 (2004).
[13] P. A. Marcos, M. J. Lopez, A. Rubio, and J. Alonso, Chem. Phys. Lett. **273**, 367 (1997).
[14] A. Perez-Garrido, J. Phys.: Condens. Matter **14**, 5077 (2002).
[15] C. P. Ewels, M. J. Heggie, and P. R. Briddon, Chem. Phys. Lett. **351**, 178 (2002).
[16] M. Bonn, S. Funk, Ch. Hess, D. N. Denzler, C. Stampfl, M. Scheffler, M. Wolf, and G. Ertl, Science **285**, 1042 (1999).
[17] M. Dürr, A. Biedermann, Z. Hu, U. Höfer, and T. F. Heinz, Science **296**, 1838 (2002).
[18] S. K. Sundaram and E. Mazur, Nat. Mater. **1**, 217 (2002).
[19] L. Bartels, F. Wang, D. Möller, E. Knoesel, and T. F. Heinz, Science **305**, 648 (2004).
[20] H. O. Jeschke, M. E. Garcia, and K. H. Bennemann, Phys. Rev. Lett. **87**, 015003 (2001).
[21] B. Torralva, T. A. Niehaus, M. Elstner, S. Suhai, T. Frauenheim, and R. E. Allen, Phys. Rev. B **64**, 153105 (2001).
[22] D. H. Reitze, H. Ahn, and M. C. Downer, Phys. Rev. B **45**, 2677 (1992).
[23] P. L. Silvestrelli, A. Alavi, M. Parrinello, and D. Frenkel, Phys. Rev. Lett. **77**, 3149 (1996).
[24] K. Sokolowski-Tinten, J. Bialkowski, A. Cavalleri, D. von der Linde, A. Oparin, J. Meyer-ter-Vehn, and S. I. Anisimov, Phys. Rev. Lett. **81**, 224 (1998).
[25] S. I. Ashitkov, M. B. Agranat, P. S. Kondratenko, S. I. Anisimov, V. E. Fortov, V. V. Temnov, K. Sokolowski-Tinten, P. Zhou, and D. von der Linde, JETP Lett. **75**, 87 (2002).
[26] H. O. Jeschke and M. E. Garcia, *Nonlinear Optics, Quantum Optics and Ultrafast Phenomena with X-rays*, edited by Bernhard W. Adams (Kluwer Academic Publishers, Boston, 2003).
[27] H. O. Jeschke, M. E. Garcia, and K. H. Bennemann, Phys. Rev. B **60**, R3701 (1999).
[28] G. P. Zhang and T. F. George, Phys. Rev. Lett. **93**, 147401 (2004).
[29] A. H. Romero, M. E. Garcia, F. Valencia, H. Terrones, M. Terrones, and H. O. Jeschke, Nano Lett. **5**, 1361 (2005).
[30] P. L. Silvestrelli and M. Parrinello, J. Appl. Phys. **83**, 2478 (1998).
[31] C. Z. Wang, K. M. Ho, M. D. Shirk, and P. A. Molian, Phys. Rev. Lett. **85**, 4092 (2000).
[32] C. H. Xu, C. Z. Wang, C. T. Chan, and K. M. Ho, J. Phys.: Condens. Matter **4**, 6047 (1992).
[33] J. Kono, G. N. Ostojic, S. Zaric, M. S. Strano, V. C. Moore, J. Shaver, R. H. Hauge, and R. E. Smalley, Appl. Phys. A **78**, 1093 (2004).
[34] A. D. Becke, Phys. Rev. A **38**, 3098 (1988).
[35] C. Lee, W. Yang, and R. G. Parr, Phys. Rev. B **37**, 785 (1988).
[36] CPMD, Copyright IBM Corp. 1990-2006, Copyright MPI für Festkörperforschung Stuttgart 1997–2001.
[37] G. Henkelman, B. P. Uberuaga, and H. Jónsson, J. Chem. Phys. **113**, 9901 (2000).
[38] G. Henkelman and H. Jónsson, J. Chem. Phys. **113**, 9978 (2000).
[39] C. H. Xu, C. L. Fu, and D. F. Pedraza, Phys. Rev. B **48**, 13273 (1993).
[40] C. P. Ewels, R. H. Telling, A. A. El-Barbary, M. I. Heggie, and P. R. Briddon, Phys. Rev. Lett. **91**, 025505 (2003).
[41] V. H. Crespi, M. L. Cohen, and A. Rubio, Phys. Rev. Lett. **79**, 2093 (1997), and references therein.
[42] B. C. Pan, W. S. Yang, and J. Yang, Phys. Rev. B **62**, 12652 (2000).
[43] H. O. Jeschke, M. E. Garcia, and K. H. Bennemann, J. Appl. Phys. **91**, 18 (2002).
[44] M. E. Garcia, T. Dumitrica, and H. O. Jeschke, Appl. Phys. A **79**, 855 (2004).
[45] Y. Miyamoto, A. Rubio, S. Berber, M. Yoon, and D. Tománek, Phys. Rev. B **69**, 121413(R) (2004).
[46] *Wavelets in Physics*, edited by J. C. van den Berg (Cambridge University Press, Cambridge, England 1999).
[47] A. Rahaman and R. A. Wheeler, J. Chem. Theory Comput. **1**, 769 (2005).
[48] A. Graps, AN INTRODUCTION TO WAVELETS (Institute of Electrical and Electronics Engineers, Houston, Texas, 1995), available online at http://www.amara.com/IEEEwave/IEEEwavelet.html
[49] D. Sanchez-Portal, E. Artacho, J. M. Soler, A. Rubio, and P. Ordejon, Phys. Rev. B **59**, 12678 (1999).
[50] H. O. Jeschke, M. E. Garcia, and J. A. Alonso, Chem. Phys. Lett. **352**, 154 (2002).